

Drude-like Thermal Hall Resistivity in the Cuprates

Liuke Lyu¹ and William Witczak-Krempa^{1,2,3}

¹*Département de Physique, Université de Montréal, Montréal, Québec, H3C 3J7, Canada*

²*Institut Courtois, Université de Montréal, Montréal (Québec), H2V 0B3, Canada*

³*Centre de Recherches Mathématiques, Université de Montréal, Montréal, QC, Canada, HC3 3J7*
(Dated: July 7, 2022)

The thermal Hall effect, which arises when heat flows transverse to an applied thermal gradient, has become an important observable in the study of quantum materials. Recent experiments found a large thermal Hall conductivity κ_{xy} in many cuprates, including deep inside the Mott insulator. Here, we uncover a surprising linear temperature dependence for the inverse thermal Hall resistivity, $1/\varrho_H = -\kappa_{xx}^2/\kappa_{xy}$, in the Mott insulating cuprates La_2CuO_4 and $\text{Sr}_2\text{CuO}_2\text{Cl}_2$. We also find this linear scaling in the pseudogap state of hole-doped Nd-LSCO in the out-of-plane direction, highlighting the importance of phonons. On the electron-doped side, the linear inverse thermal Hall signal emerges in NCCO and PCCO at various dopings, including in the strange metal. Although such dependence arises in the simple Drude model for itinerant electrons, its origin is unclear in strongly correlated Mott insulating or pseudogap states. We perform a Boltzmann analysis for heat carriers, such as phonons, incorporating skew-scattering, and we are able to identify regimes where a linear T inverse Hall resistivity appears. Finally, we suggest future experiments on various materials that would further our fundamental understanding of heat transport in quantum materials.

Introduction—The thermal Hall effect occurs when a system is subjected to a temperature gradient that results in a flow of heat in the transverse direction, in analogy to the electrical Hall effect. Due to its ability to detect neutral excitations, it has recently been used to probe quantum spin liquid candidate materials [1, 2], and to provide experimental evidence for the elusive Majorana fermions in topological states of matter that are insulating in their bulk [3, 4]. Subsequent experiments found an unexpected large thermal Hall effect in a wider variety of insulators, such as the cuprate Mott insulators La_2CuO_4 and $\text{Sr}_2\text{CuO}_2\text{Cl}_2$, the quantum paraelectric SrTiO_3 , and the cubic antiferromagnetic insulator Cu_3TeO_6 [5–8]. The temperature dependences of the longitudinal thermal conductivity κ_{xx} and transverse (or Hall) thermal conductivity κ_{xy} are often shown; with their ratio κ_{xy}/κ_{xx} quantifying the relative magnitude of the thermal Hall effect. Recent theoretical works [9, 10] have suggested that the *thermal Hall resistivity* $\varrho_H \equiv -\kappa_{xy}/\kappa_{xx}^2$ is often simpler to interpret than κ_{xy}/κ_{xx} . Physically, the thermal Hall resistivity $\varrho_H = \nabla_y T/J_x$ represents the transverse temperature gradient due to a given longitudinal heat flux. One motivation to study this quantity comes from the observation that extrinsic mechanisms for the thermal Hall effect usually predict

$$\kappa_{xx} \sim \tau, \quad \kappa_{xy} \sim \tau^2 \quad (1)$$

where τ is the total relaxation time, which thus cancels out in ϱ_H (see for example [11]). Since τ can be sample-dependent and difficult to model, it is advantageous to study a quantity independent of τ . In this work, we find that the inverse thermal Hall resistivity ϱ_H^{-1} possesses a simple dependence on temperature in a wide variety of cuprates.

We first begin by showing that the experiments for the cuprates show a linear inverse thermal Hall resistivity

$\varrho_H^{-1} \approx AT$ in various undoped, hole-doped, and electron-doped materials. We also find that ϱ_H^{-1} scales inversely with the applied field for an electron-doped cuprate. We then explain how such temperature and field scaling appears in the simple Drude model for itinerant electrons. Given the inapplicability of such a model to the cuprates, we study a kinetic Boltzmann equation for heat carriers, such as phonons. Under certain assumptions that we motivate, we uncover a linear scaling in agreement with experiments. We end with a discussion of the implications of our findings, outlining future experiments in various materials to investigate the conditions for such striking linear scaling.

Thermal Hall resistivity for the cuprates—We now examine the experimental data for ϱ_H in various cuprates. The first group of materials includes the undoped cuprate Mott insulators La_2CuO_4 (LCO) and $\text{Sr}_2\text{CuO}_2\text{Cl}_2$ (SCOC) with a similar crystal structure and antiferromagnetic order. Both materials contain layered copper-oxygen planes, where the Cu^{2+} moments form a 2D antiferromagnet with a Néel temperature $T_N \approx 300$ K (La) and 250 K (Sr), respectively [12]. Below 530 K, La_2CuO_4 has an orthorhombic structure with spins slightly canting out of the CuO_2 plane, while $\text{Sr}_2\text{CuO}_2\text{Cl}_2$ remain in tetragonal structure down to at least 10 K [12]. We found that ϱ_H^{-1} scales linearly with T over a wide range of temperatures:

$$\varrho_H^{-1} = -\frac{\kappa_{xx}^2}{\kappa_{xy}} \approx AT + A_0 \quad (2)$$

as shown in Fig. 1. This is remarkable given that the longitudinal and transverse thermal conductivities possess non-monotonic temperature dependence (Fig. 1), with maxima at different temperatures. This shows that a hitherto undiscovered correlation exists between κ_{xx} and κ_{xy} .

In order to better understand the role of phonons in

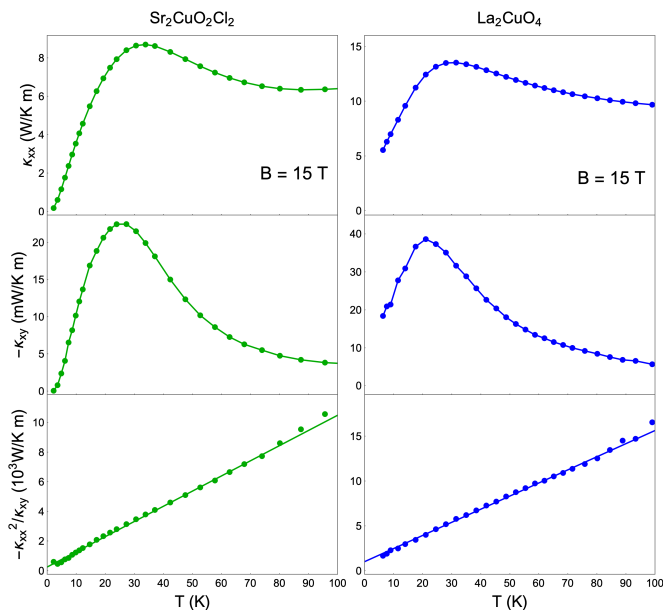


FIG. 1. Thermal longitudinal conductivity (top), Hall conductivity (middle), and inverse thermal Hall resistivity $\varrho_H^{-1} = -\kappa_{xx}^2/\kappa_{xy}$ (bottom) for the cuprate Mott insulators SCOC and LCO. The bottom plots show a linear fit, $AT + A_0$, with $A^{\text{La/Sr}} = 0.15, 0.10 \times 10^3 \text{ W}/(\text{K}^2 \text{ m})$, $A_0^{\text{La/Sr}} = 0.95, 0.25 \times 10^3 \text{ W}/(\text{K m})$. Data from [6].

the linear scaling (2) compared to electronic excitations, including magnons, we now examine thermal transport along the c -axis. We find that the linear scaling (2) is also present in the pseudogap phase of $\text{La}_{1.6-x}\text{Nd}_{0.4}\text{Sr}_x\text{CuO}_4$ (Nd-LSCO) at hole doping $p = 0.21$. As shown in Fig. 2, the c -axis inverse thermal Hall resistivity is linear in a wide range of temperatures above 20 K. This shows that the linear behavior (2) is present not only beyond the Mott insulating regime but also perpendicular to the CuO planes, which points to the central role of phonons in the effect. We note that the magnitude of ϱ_H^{-1} is smaller by a factor of 10 compared with the undoped cuprates.

We now turn to electron-doped cuprate $\text{Nd}_{2-x}\text{Ce}_x\text{CuO}_4$ (NCCO). At doping $x = 0.04$, the sample is in the antiferromagnetic Mott insulating phase. We see that both κ_{xx} and κ_{xy}/B are suppressed with increasing field (Fig. 3 left, top/middle). The latter implies a marked sub-linear scaling of the thermal Hall conductivity [14]. In contrast, the inverse thermal Hall coefficient $R_{\text{TH}}^{-1} = B\varrho_H^{-1}$ (Fig. 3 left bottom) remains virtually the same for the three field values and increases linearly with temperature beyond 50 K. In that range, ϱ_H^{-1} thus shows a T/B dependence; we will see below that dependence also appears in the Drude model. Next, at $x = 0.17$, which is above optimal doping, the sample is in the superconducting phase at zero magnetic field with $T_c = 6 \text{ K}$ [15]. Upon applying a 15 T magnetic field, superconductivity disappears and leaves behind a non-Fermi liquid [16]. As shown in the right

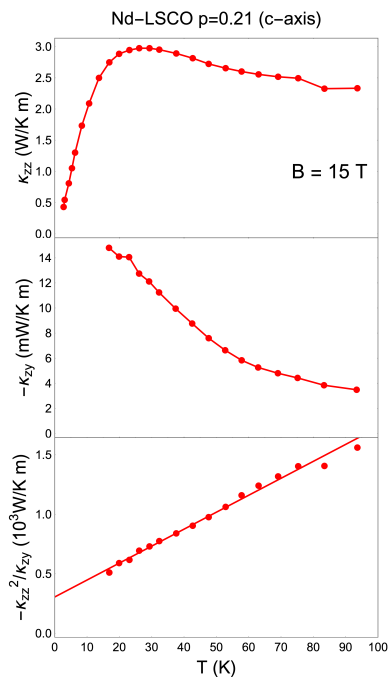


FIG. 2. Thermal conductivities (top and middle), and ϱ_H^{-1} (bottom) along the c -axis versus temperature for the hole-doped cuprate Nd-LSCO at doping $p = 0.21$. The linear fit corresponds to $A = 0.014 \times 10^3 \text{ W}/(\text{K}^2 \text{ m})$, and $A_0 = 0.32 \times 10^3 \text{ W}/(\text{K m})$. Data from [13].

column of Fig. 3, ϱ_H^{-1} scales linearly with T until 60 K. Interestingly, the linear regime ends at the temperature where it begins for 0.04 doping, distinguishing the Mott insulator and pseudogap states.

$\text{Pr}_{2-x}\text{Ce}_x\text{CuO}_4$ (PCCO) is another electron-doped cuprate closely related to NCCO. At doping $x = 0.15$ and zero field, PCCO becomes superconducting at $T_c \approx 20 \text{ K}$ [17]. In the metallic phase at 15 T, the inverse thermal Hall resistivity (see Appendix Fig. 5) shows a similar temperature dependence to NCCO, but the deviation from linearity happens at a lower temperature $\sim 40 \text{ K}$. By using the electrical Hall conductivity, an estimate of the electronic contribution κ_{xy}^e was obtained by assuming the Wiedemann-Franz law [14]. At low temperature ($T < 40 \text{ K}$), κ_{xy}^e is seen to be of opposite sign and much smaller in magnitude than the measured thermal Hall conductivity (less than 10%). It would be interesting to investigate the extent of the linear regime as a function of doping. Before moving to the theoretical description, we note that the slope A in the electron-doped cuprates is of similar magnitude to what was found for the undoped Mott insulators LCO and SCOC, $A \sim 10^2 \text{ W}/(\text{K}^2 \text{ m})$.

Drude model—Before turning to a more realistic description for the thermal transport in the cuprates, we point out that the simple Drude model for itinerant electrons (or holes) shows this exact temperature dependence for the thermal Hall resistivity (2). For an electron gas in a uniform magnetic field B , the Drude longitudinal and

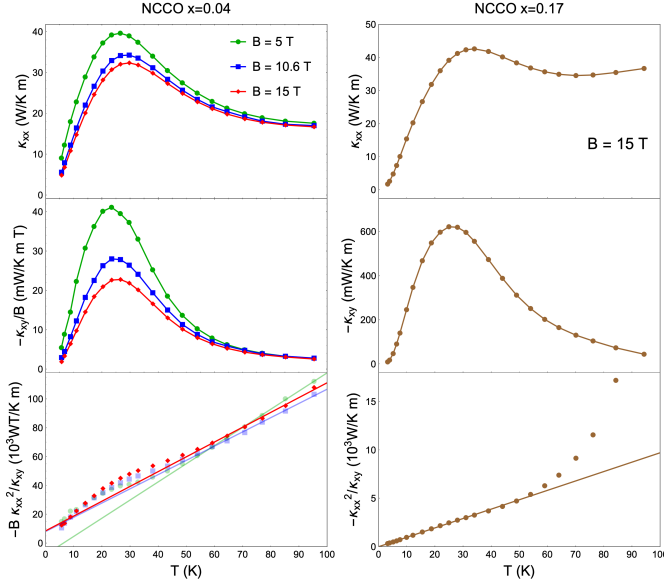


FIG. 3. Thermal conductivities (top and middle), and ϱ_H^{-1} (bottom) versus temperature for the electron-doped cuprate NCCO at doping $x = 0.04$ (left) and 0.17 (right). In the left column, where $T \geq 5$ K, we see that κ_{xy}/B strongly depends on the applied field B , but the inverse thermal Hall coefficient $R_{\text{TH}}^{-1} = B/\varrho_H$ shows a much weaker field dependence. The linear fit for $B = 5, 10.6, 15$ T gives $A = 0.26, 0.09, 0.07 \times 10^3 \text{W}/(\text{K}^2\text{m})$, and $A_0 = -1.56, 0.77, 0.57 \times 10^3 \text{W}/(\text{K}\text{m})$. On the right column, the fit corresponds to $A = 0.10 \times 10^3 \text{W}/(\text{K}^2\text{m})$, and $A_0 = 0.002 \times 10^3 \text{W}/(\text{K}\text{m})$. Data from [14].

transverse electrical conductivities are

$$\sigma_{xx} = \frac{nq^2\tau}{m}, \quad \sigma_{xy} = -\omega_c\tau\sigma_{xx}, \quad \frac{\sigma_{xx}^2}{-\sigma_{xy}} = \frac{nq}{B} \quad (3)$$

where $\omega_c = qB/m$ is the cyclotron frequency, q is the electric charge, n is the charge carrier number density, m is the effective mass, and τ is the elastic scattering time. A key observation is that $-\sigma_{xx}^2/\sigma_{xy}$ is independent of τ and thus independent of temperature. Now, the Wiedemann-Franz law relates the thermal and electrical conductivities: $\kappa = L\sigma T$, where $L = \frac{\pi^2}{3}(k_B/e)^2$ is the Lorenz number, so that we can relate the thermal ratio (2) to the corresponding one for charge conductivities:

$$\varrho_H^{-1} = \frac{\kappa_{xx}^2}{-\kappa_{xy}} = \frac{(L\sigma_{xx}T)^2}{-L\sigma_{xy}T} = L\frac{nq}{B}T \quad (4)$$

We thus recover a linear in T inverse thermal Hall resistivity. We note in passing that in order to obtain the same sign as in Figs. 1-3, the carriers should be holes ($q > 0$). However, the arguments leading to (4) cannot be applied to Mott insulators where the electric charge is localized at low temperatures. The dominant heat carriers in cuprate Mott insulators ought to be phonons, and to a lesser extent magnons. Some recent works discussed the possibility of chiral transport by phonons due to skew

scattering, and we now examine how it can give rise to the linear relation (2).

Boltzmann Analysis—We begin with the Boltzmann equation for bosonic heat carriers:

$$\frac{\partial f_{\mathbf{k}}}{\partial \omega_{\mathbf{k}}} \omega_{\mathbf{k}} \frac{\mathbf{v}_{\mathbf{k}} \cdot \nabla T}{T} = \frac{\delta f_{\mathbf{k}} + \delta f'_{\mathbf{k}}}{\tau(\omega_{\mathbf{k}})} + \int d^3\mathbf{k}' [1 + 2\bar{f}_{\mathbf{k}}] (W_{\mathbf{k}'\mathbf{k}}^A \delta f_{\mathbf{k}} - W_{\mathbf{k}\mathbf{k}'}^A \delta f_{\mathbf{k}'}) \quad (5)$$

where $\omega_{\mathbf{k}}, \mathbf{v}_{\mathbf{k}}$ are the heat carrier frequency and velocity, respectively. $f_{\mathbf{k}}$ is the non-equilibrium heat carrier distribution, which we divide into three components: $f_{\mathbf{k}} = \bar{f}_{\mathbf{k}} + \delta f_{\mathbf{k}} + \delta f'_{\mathbf{k}}$. The first term \bar{f} represents the equilibrium distribution, which does not carry current. The second term is the longitudinal perturbation $\delta f \propto \nabla_x T$ driven by the applied temperature gradient, taken to be along x . The third term is a skew distribution $\delta f' \propto B \nabla_x T$ proportional to both the temperature gradient and the magnetic field. We use the following skew-scattering term [18]: $W_{\mathbf{k}\mathbf{k}'}^A = \Omega \hat{z} \cdot (\hat{k} \times \hat{k}') \delta(\omega_{\mathbf{k}} - \omega_{\mathbf{k}'})$, where we have taken the magnetic field to be along the z -axis; $\Omega \hat{z}$ is a ‘‘Berry curvature’’-term proportional to the applied magnetic field. We now introduce the skew scattering rate into mode \mathbf{k} :

$$\tau_{s,\mathbf{k}}^{-1} = \int d^3\mathbf{k}' (\hat{v}_{\mathbf{k}} \cdot \hat{y}) W_{\mathbf{k}\mathbf{k}'}^A (\hat{v}_{\mathbf{k}'} \cdot \hat{x}) = \frac{k^2 \Omega(k)}{v_k} \int_{S^2} d^2\hat{k}' (\hat{v}_{\mathbf{k}} \cdot \hat{y}) \hat{z} \cdot (\hat{k} \times \hat{k}') (\hat{v}_{\mathbf{k}'} \cdot \hat{x}) \quad (6)$$

where the integral is over the unit sphere. The thermal Hall conductivity is then

$$\kappa_{xy} = - \int \frac{d^3\mathbf{k}}{(2\pi)^3} v^2 \frac{\omega^2}{T} \frac{\partial \bar{f}}{\partial \omega} \tau^2 \tau_{s,\mathbf{k}}^{-1} [1 + 2\bar{f}(\omega)] \quad (7)$$

At low temperature, and assuming that both skew and non-skew scattering rates have a power-law dependence on frequency, we can simplify the heat conductivities (see also [11])

$$\kappa_{xx} = \frac{C}{3} v^2 \tau, \quad \kappa_{xy} = \frac{C}{3} v^2 \tau^2 \tau_s^{-1}, \quad \frac{\kappa_{xx}^2}{\kappa_{xy}} = \frac{C}{3} v^2 \tau_s, \quad (8)$$

where C is the specific heat, τ^{-1} is the longitudinal scattering rate and τ_s^{-1} is the total skew-scattering rate derived from $\tau_{s,\mathbf{k}}^{-1}$. If we assume $\tau_{s,\mathbf{k}}^{-1} \propto k^m$, then $\tau_s^{-1} \propto T^m$ at low temperatures. Combining Eqs. (2) and (8), we see that the product $C\tau_s = (3A/v^2)T$ should be linear in T . For a low-temperature Debye heat capacity $C \propto T^3$ we should have $\tau_s^{-1} \propto T^2$, and $m = 2$. This gives $\tau_{s,\mathbf{k}}^{-1} \propto k^2$, and correspondingly Ω is frequency independent. However, the specific heat of the cuprates is expected to deviate from T^3 in the temperature range where the linearity of ϱ_H^{-1} emerges. Indeed, experiments on La_2CuO_4 showed that the heat capacity is roughly T^3 below 20 K (estimated from $\text{La}_2\text{CuO}_{4.093}$), but becomes linear between 20 and 60 K [19, 20]. Therefore,

a more realistic possibility in the intermediate temperature regime is that $C \propto T$, and that τ_s^{-1} is temperature independent.

The kinetic equation result (8) predicts a linear magnetic field dependence for the thermal Hall resistivity $\varrho_H \propto B/T$, just as in the Drude model. This is in agreement with the B -linear scaling observed for NCCO, Fig. 3.

Discussion— To summarize, we have discovered a linear temperature dependence of the inverse thermal Hall resistivity in a set of undoped, electron-doped, and hole-doped cuprates which exhibit a large thermal Hall effect. In the case of Nd-LSCO, the linearity holds when the heat gradient is applied orthogonal to the CuO planes, in line with previous claims that chiral phonons are responsible for thermal Hall effect in cuprates [13]. Although the well-known Drude model of itinerant electrons obeys the linear relation (2), it cannot be applied to the cases that we studied, which range from the Mott insulating phase to the pseudogap. Instead, we found that a Boltzmann transport equation for phonons (and other bosonic excitations), under reasonable conditions, gives rise to linearity for ϱ_H^{-1} . It also yields a $1/B$ dependence with respect to the magnetic field, so we have $\varrho_H^{-1} \propto T/B$. An important step forward would be to identify the microscopic origin of the skew-scattering collision term in the Boltzmann equation, and to better understand the role of other excitations such as magnons. Further specific heat measurements would be needed to shed light on the skew-scattering rate appearing in the kinetic treatment, Eq. (8).

Interestingly, the linear dependence over a wide range of temperatures (2) is not present in all undoped Mott insulators. For the cuprate Nd_2CuO_4 , the linearity is present up to 20 K, at which point ϱ_H^{-1} reaches a maximum, and increases until reaching a second linear regime at 70 K (see Appendix Fig.4). The deviation from the linearity observed in LCO and SCOC, Fig.1, could arise from additional scattering in the longitudinal direction, which can be seen from a sharper decrease of κ_{xx} (see

Appendix Fig. 4). Compared with the other two Mott insulators, Nd_2CuO_4 possesses certain distinct features. First, κ_{xx} is more sensitive to the external field. This may result from additional spin-phonon scattering, which is more prominent in Nd_2CuO_4 due to a large magnetic moment carried by the Nd^{3+} sites [21]. Nd_2CuO_4 also has spin reorientations between successive CuO layers at 30 K and 70 K both without and with field [22, 23], which roughly matches the range where ϱ_H^{-1} deviates from linearity. To examine this effect, future experiments may compare Nd_2CuO_4 with its sister compounds such as Pr_2CuO_4 and Sm_2CuO_4 which do not show such spin reorientations.

A large thermal Hall conductivity was also found in the mixed state of $\text{YBa}_2\text{Cu}_3\text{O}_{6+x}$ (YBCO) at $x = 1$ below $T_c = 89$ K, which was attributed to the asymmetric scattering of quasiparticles by pinned vortices [24]. The magnitude of the Hall effect was roughly $\kappa_{xy}/\kappa_{xx} \sim 1\%$, which is comparable with the NCCO data in Fig. 3. It was claimed that κ_{xy} was dominated by the quasiparticles. Given the new understanding of chiral phonons in the cuprates, it would be desirable to revisit the thermal Hall effect in YBCO as a function of doping, both in- and out-of-plane, in particular, to see whether the thermal Hall resistivity possesses a linear- T regime. Interestingly, a T -linear relation was observed for the inverse *electrical* Hall coefficient R_H^{-1} above T_c at various dopings in YBCO [25]. It remains unclear whether this bears any relation to the thermal case, Eq. (2).

On the experimental side, our work motivates the analysis of the thermal conductivities in more materials to understand the universality of the linear inverse thermal Hall resistivity. In addition, the linear scaling (2) gives a simple yet stringent constraint on theoretical models.

Acknowledgment.— We thank L. Taillefer and G. Grissonnanche for key suggestions and comments. We also thank R. Boyack for helpful discussions, and L. Chen and M.-E. Boulanger for providing the experimental data. This research was funded by a Team Research Project from FRQNT, a Discovery Grant from NSERC, a Canada Research Chair, and a grant from the Fondation Courtois.

-
- [1] M. Hirschberger, J. W. Krizan, R. J. Cava, and N. P. Ong, Large thermal hall conductivity of neutral spin excitations in a frustrated quantum magnet, *Science* **348**, 106 (2015), <https://www.science.org/doi/pdf/10.1126/science.1257340>.
- [2] K. Sugii, M. Shimozawa, D. Watanabe, Y. Suzuki, M. Halim, M. Kimata, Y. Matsumoto, S. Nakatsuji, and M. Yamashita, Thermal hall effect in a phonon-glass $\text{Ba}_3\text{CuSb}_2\text{O}_9$, *Phys. Rev. Lett.* **118**, 145902 (2017).
- [3] M. Banerjee, M. Heiblum, V. Umansky, D. E. Feldman, Y. Oreg, and A. Stern, Observation of half-integer thermal Hall conductance, *Nature (London)* **559**, 205 (2018), [arXiv:1710.00492 \[cond-mat.mes-hall\]](https://arxiv.org/abs/1710.00492).
- [4] Y. Kasahara, T. Ohnishi, Y. Mizukami, O. Tanaka, S. Ma, K. Sugii, N. Kurita, H. Tanaka, J. Nasu, Y. Motome, T. Shibauchi, and Y. Matsuda, Majorana quantization and half-integer thermal quantum Hall effect in a Kitaev spin liquid, *Nature (London)* **559**, 227 (2018), [arXiv:1805.05022 \[cond-mat.str-el\]](https://arxiv.org/abs/1805.05022).
- [5] G. Grissonnanche, A. Legros, S. Badoux, E. Lefrançois, V. Zlatko, M. Lizaire, F. Laliberté, A. Gourgout, J. S. Zhou, S. Pyon, T. Takayama, H. Takagi, S. Ono, N. Doiron-Leyraud, and L. Taillefer, Giant thermal hall conductivity in the pseudogap phase of cuprate superconductors, *Nature* **571**, 376 (2019).
- [6] M.-E. Boulanger, G. Grissonnanche, S. Badoux, A. Al-

- laire, E. Lefrançois, A. Legros, A. Gourgout, M. Dion, C. Wang, and X. Chen, Thermal hall conductivity in the cuprate mott insulators Nd_2CuO_4 and $\text{Sr}_2\text{CuO}_2\text{Cl}_2$, *Nature communications* **11**, 1 (2020).
- [7] X. Li, B. Fauqué, Z. Zhu, and K. Behnia, Phonon thermal hall effect in strontium titanate, *Physical review letters* **124**, 105901 (2020).
- [8] L. Chen, M.-E. Boulanger, Z.-C. Wang, F. Tafti, and L. Taillefer, Large phonon thermal hall conductivity in a simple antiferromagnetic insulator (2021), arXiv:2110.13277 [cond-mat.str-el].
- [9] L. Mangeolle, L. Balents, and L. Savary, Thermal conductivity and theory of inelastic scattering of phonons by collective fluctuations (2022), arXiv:2202.10366 [cond-mat.str-el].
- [10] H. Guo, D. G. Joshi, and S. Sachdev, Resonant thermal hall effect of phonons coupled to dynamical defects (2022).
- [11] X.-Q. Sun, J.-Y. Chen, and S. A. Kivelson, Large extrinsic phonon thermal hall effect from resonant scattering (2021).
- [12] D. Vaknin, S. K. Sinha, C. Stassis, L. L. Miller, and D. C. Johnston, Antiferromagnetism in $\text{Sr}_2\text{CuO}_2\text{Cl}_2$, *Phys. Rev. B* **41**, 1926 (1990).
- [13] G. Grissonnanche, S. Thériault, A. Gourgout, M.-E. Boulanger, E. Lefrançois, A. Ataei, F. Laliberté, M. Dion, J.-S. Zhou, S. Pyon, T. Takayama, H. Takagi, N. Doiron-Leyraud, and L. Taillefer, Chiral phonons in the pseudogap phase of cuprates, *Nature Physics* **16**, 1108 (2020).
- [14] M.-E. Boulanger, G. Grissonnanche, E. Lefrançois, A. Gourgout, K.-J. Xu, Z.-X. Shen, R. L. Greene, and L. Taillefer, Thermal hall conductivity of electron-doped cuprates, *Phys. Rev. B* **105**, 115101 (2022).
- [15] T. Helm, M. V. Kartsovnik, M. Bartkowiak, N. Bittner, M. Lambacher, A. Erb, J. Wosnitzer, and R. Gross, Evolution of the fermi surface of the electron-doped high-temperature superconductor $\text{Nd}_{2-x}\text{Ce}_x\text{CuO}_4$ revealed by shubnikov-de haas oscillations, *Phys. Rev. Lett.* **103**, 157002 (2009).
- [16] M. Lambacher, *Crystal growth and normal state transport of electron doped high temperature superconductors*, Thesis, Technical University of Munich (2008).
- [17] H. Takagi, S. Uchida, and Y. Tokura, Superconductivity produced by electron doping in CuO_2 -layered compounds, *Phys. Rev. Lett.* **62**, 1197 (1989).
- [18] J.-Y. Chen, S. A. Kivelson, and X.-Q. Sun, Enhanced thermal hall effect in nearly ferroelectric insulators, *Phys. Rev. Lett.* **124**, 167601 (2020).
- [19] T. Hirayama, M. Nakagawa, and Y. Oda, Observation of specific heat jump in $\text{La}_2\text{CuO}_{4.093}$ due to superconducting transition, *Solid State Communications* **113**, 121 (1999).
- [20] G. A. Jorge, M. Jaime, L. Civale, C. D. Batista, B. L. Zink, F. Hellman, B. Khaykovich, M. A. Kastner, Y. S. Lee, and R. J. Birgeneau, Thermodynamic properties of excess-oxygen-doped $\text{La}_2\text{CuO}_{4.11}$ near a simultaneous transition to superconductivity and long-range magnetic order, *Phys. Rev. B* **69**, 174506 (2004).
- [21] S. Y. Li, L. Taillefer, C. H. Wang, and X. H. Chen, Ballistic magnon transport and phonon scattering in the antiferromagnet Nd_2CuO_4 , *Phys. Rev. Lett.* **95**, 156603 (2005).
- [22] S. Skanthakumar, H. Zhang, T. Clinton, W.-H. Li, J. Lynn, Z. Fisk, and S.-W. Cheong, Magnetic phase transitions and structural distortion in Nd_2CuO_4 , *Physica C: Superconductivity* **160**, 124 (1989).
- [23] S. Li, S. D. Wilson, D. Mandrus, B. Zhao, Y. Onose, Y. Tokura, and P. Dai, *Physical Review B* **71**, 054505 (2005).
- [24] K. Krishana, J. M. Harris, and N. P. Ong, Quasiparticle mean free path in $\text{YBa}_2\text{Cu}_3\text{O}_7$ measured by the thermal hall conductivity, *Phys. Rev. Lett.* **75**, 3529 (1995).
- [25] R. Jin and H. R. Ott, Hall effect of $\text{YBa}_2\text{Cu}_3\text{O}_{7-\delta}$ single crystals, *Phys. Rev. B* **57**, 13872 (1998).
- [26] T. Chattopadhyay, P. Brown, and U. Köbler, Crystal and magnetic structure of Nd_2CuO_4 at millikelvin temperatures, *Physica C: Superconductivity* **177**, 294 (1991).
-

Appendix A: Thermal conductivity data for additional cuprates

Mott insulating NCO— Nd_2CuO_4 is another undoped cuprate Mott insulator with a tetragonal crystal structure. Similar to LCO and SCOC, Nd_2CuO_4 has quasi-2D antiferromagnetic order, with Néel temperature $T_N = 245$ K [26]. The bottom panel of Fig. 4 shows a clear deviation from linearity between 20 – 70 K, which roughly corresponds to the spin reorientation range 30 – 85 K. Further analysis is required to explain this deviation.

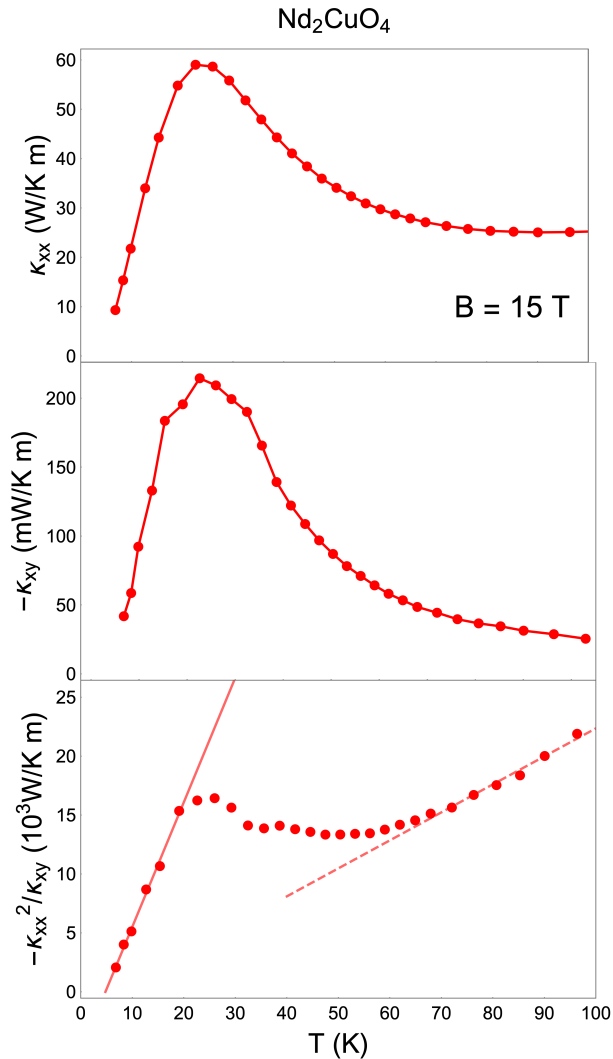


FIG. 4. Thermal conductivities (top and middle), and ϱ_H^{-1} versus temperature for undoped cuprate Mott insulator Nd_2CuO_4 . We see a deviation from linearity between 20 and 70 K. The low- T linear fit (solid line) corresponds to $A = 1.1 \times 10^3 \text{W}/(\text{K}^2\text{m})$ and $A_0 = -5.0 \times 10^3 \text{W}/(\text{Km})$, while the high- T linear fit (dashed line) corresponds to $A = 0.24 \times 10^3 \text{W}/(\text{K}^2\text{m})$ and $A_0 = -1.4 \times 10^3 \text{W}/(\text{Km})$. Data from [6].

Electron-doped cuprate PCCO— $\text{Pr}_{2-x}\text{Ce}_x\text{CuO}_4$ (PCCO) at doping $x = 0.15$ satisfies the linear relation $\varrho_H^{-1} = AT + A_0$ in the range 5 – 40 K with the same slope A as NCCO at doping $x = 0.17$ (Fig. 3). The non-linear dependence starting at 40 K roughly corresponds with the onset of an additional contribution to κ_{xx} .

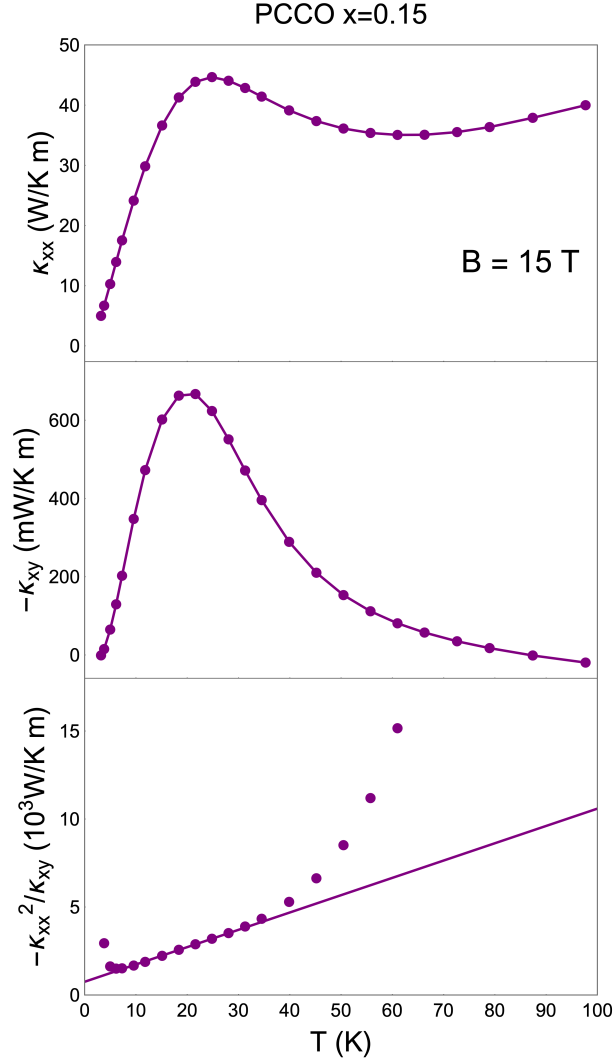


FIG. 5. Thermal conductivities (top and middle), and ϱ_H^{-1} versus temperature for electron-doped cuprate $\text{Pr}_{2-x}\text{Ce}_x\text{CuO}_4$ (PCCO). We see a deviation from linearity at around 40 K. The linear fit corresponds to $A = 0.10 \times 10^3 \text{W}/(\text{K}^2\text{m})$ and $A_0 = 0.67 \times 10^3 \text{W}/(\text{Km})$. Data from [14].